

Extrasolar and Bl Lac observations at OARPAF

C. RIGHI⁽¹⁾⁽²⁾

⁽¹⁾ *Università degli Studi dell'Insubria - via Valleggio 11, I-22100, Como, Italy*

⁽²⁾ *INAF-Osservatorio Astronomico di Brera - via Bianchi 46, I-23807, Merate (LC), Italy*

received 3 February 2016

Summary. — This paper reports the work done at the Osservatorio Astronomico Regionale Parco Antola comune di Fascia (OARPAF), as a part of my master thesis. The paper is divided in three parts: the first part describes the instrumentation at the OARPAF; the second part shows the characterization of the instrumentation, from the pointing model of the telescope to the conception and the realization of the software for data analysis; the third part illustrates the results of the photometric calibration.

1. – Introduction

The OARPAF (or Antola Observatory) [1] is located near Genova, Italy, at 1487 m above sea level, and it has been in regular operation since October 2011. The OARPAF is equipped with a 0.8 m, $F/8$ telescope designed by the Astelco company⁽¹⁾ (Antola Telescope or AT/T80), with a field of view (FoV) of 20 arcmin and an Alt-Az mount in a Cassegrain-Nasmyth optical configuration which it is used for both research and outreach. The telescope is equipped with two CCD cameras: the first SBIG one is used for photometric observations using a set of Johnson-Cousin UVBVRcIc filters; the second one is paired to an Echelle spectrograph.

The University of Genoa has recently started exploiting the telescope for scientific purposes, and the first results of such efforts are outlined in my master thesis, from the commissioning and characterization of the instrumentation to the first photometric measurements. In this paper I will describe the feasibility study of the optical variability of selected astronomical objects at the Antola Observatory. Due to its characteristics, the telescope can be used to perform observations with relatively long exposure times (*e.g.* measurements of photometric variability). This paper presents the commissioning and characterization of the instrumentation as well as the calibrations, to compute the

⁽¹⁾ <http://www.astelco.com/>

response function and image quality. Then, I outline the software framework and tools (such as the exposure time calculator, or ETC, and the code for image analysis). These tools make it possible to estimate the expected performances of the instrumentation in order to prepare telescope observations, and to evaluate the quality of the collected data, as well as the experimental uncertainties.

The feasibility study aims at preparing a campaign towards the first measurement with the telescope of the Antola Observatory, using simulations that take into account both theoretical and experimental aspects.

2. – The telescope and the camera detector

The Antola telescope is a 0.8 m Alt-Az Cassegrain-Nasmyth realized by ASTELCO. In fact, the telescope has an *alt-azimuth mount* which consists of a simple two-axis mount to support and rotate the telescope around two perpendicular axes; a vertical one and a horizontal one. To use a CCD for capturing long-exposure images, a *derotator* is available. The third flat mirror of the Antola telescope can be manually rotated in two positions: the “observing flange”, for observation (with a focuser) and on the opposite side the “scientific flange”, for scientific use with the derotator. One of the two available CCD cameras, a SBIG 11000M, was used in this work. I am reporting the main features in the following section.

2.1. Readout Noise. – Readout noise is usually quoted for a CCD in terms of the number of electrons introduced per pixel into the final signal upon readout of the device. We got the following values:

CCD	$RN_{\text{exp}} [e^-]$	$RN_{\text{data sheet}} [e^-]$
SBIG 11000M	12	11

2.2. Dark current. – Dark current (DC) is the relatively small electric current that flows through photosensitive devices even when no photon is entering the device⁽²⁾. Thermal generation of electrons in silicon is a strong function of the temperature of the CCD, for this reason in astronomy CCD are generally provided with a cooling system.

Dark current for a CCD is usually specified as the number of thermal electrons generated per second per pixel or as the actual current generated per area of the device (*i.e.*, pA cm^{-2}). It is found that, in the case of SBIG 11000M, at the temperature of $T = -6^\circ\text{C}$, the value of DC is $0.69 \pm 0.06 [e^-/\text{pixel}/\text{s}]$.

2.3. Plate Scale. – The *plate scale* of a telescope can be described as the number of arcseconds corresponding to a number of pixels (or millimeters) at the focal plane of a telescope (in the grid of the CCD). So the plate scale can be determined by the distance between the detector and the primary mirror or lens (which is equal to the focal length of the mirror or lens when the image is in focus), and the size of each pixel on the CCD chip. We can determine the plate scale in terms of pixel size (s in μm) and focal length

⁽²⁾ Physically, dark current is due to the random generation of electrons and holes within the depletion region of the device that are then swept by the high electric field.

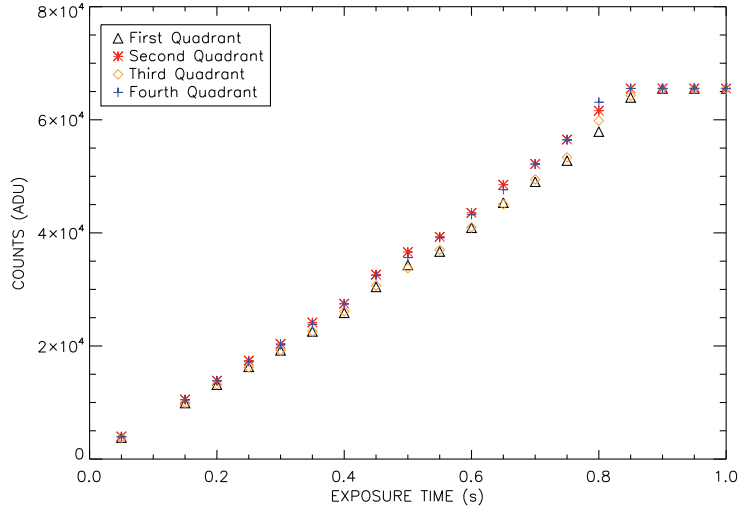


Fig. 1. – The linearity measured for the SBIG CCD camera. All frames are divided by four; this plot shows the linearity for all subframes.

(f in mm),

$$(1) \quad PS = \frac{206265 \cdot s}{f},$$

where $1/206265$ radian is equal to 1 arcsec⁽³⁾. At the Antola Observatory the focal ratio of the telescope is $F = 8$ and the diameter of the primary mirror is $D = 800$ mm; so the focal length is $f = 6400$ mm. Since for both CCD cameras the pixel size is $s = 9 \mu\text{m}$, we have a plate scale of 0.29 arcsec/pixel.

2.4. Linearity. – In this context linearity means a linear relation between the charge collected within each pixel and the digital number stored in the output image. The largest output number that a CCD can produce is set by the number of bits in the A/D converter. We have a 16 bit A/D; so it might handle numbers as large as 65 535 ADU. A linearity curve for measurements at -15°C is shown in fig. 1: the four symbols correspond to the four quadrants of the frame. The linearity is similar for all quadrants except for the high-count region.

3. – ETC

ETCs allow astronomers to predict the signal-to-noise ratio (S/N) —or, conversely, the exposure time needed to achieve a desired S/N — under a set of assumptions about the performance of an instrument and the observing conditions.

The Antola telescope Exposure Time Calculator (*AntETC*) was written thinking that observers may have a wide range of needs, so we prepared a tool as flexible as

⁽³⁾ This implies that a star with a parallax of 1 arcsec is located at a distance of 206 265 times the Astronomical Unit (AU).

TABLE I. – *The table lists all parameters used in the AntETC; the column on the left lists the fixed parameters, for which the values are hardcoded in the software; the column on the right lists the parameters for which the user is expected to provide a value.*

Fixed parameters	User-defined parameters
Quantum efficiency of CCD camera	Object (spectrum, magnitude and in some case redshift)
Telescope characteristic(reflectivity, light-collecting area, etc.)	Filter (Johnson filter)
CCD characteristic (readout noise, dark current, gain, pixel size, etc.)	Aperture photometry
Atmospheric condition (Rayleigh scattering)	Other atmospheric condition (seeing, sky brightness and air mass); point spread function (Gaussian or Moffat function); exposure parameters (detector integration time, total exposure time)

possible. In fact there is a wide choice of different model spectra available (*e.g.* different main-sequence stars). It is also possible to select a blackbody spectrum or a power-law spectrum. The software is written in Python and its interface provides an additional graphical output showing the S/N vs. exposure time. The set of fixed and user-defined parameters, listed in table II, is used to calculate the incident flux F as well as the overall efficiency factor L , which includes the transmission coefficient of the atmosphere and the acceptance of the telescope and the instruments.

If you want to determine the expected count rate from a given source, you must know the flux F . This is determined by using the input flux wavelength distribution. The user can select one out of several shapes: template spectra (star or quasar); black body; power law; SDSS Spectroscopic Data.

3.1. Main formula for signal-to-noise ratio and exposure time. – To quantify the signal-to-noise ratio (S/N), making the CCD integration time dependence explicit, we used a figure of merit of the form $S/\sqrt{S+B}$ where S and B represent the signal and background count rates, respectively:

$$(2) \quad \frac{S}{N} = \frac{N_* t}{\sqrt{(N_* + N_{\text{sky}})t + n_{\text{pixel}}(N_{\text{dark}}t + \text{RON}^2)}}.$$

In eq. (2), N_* is the *signal* term, *i.e.* the number of photons collected from the object of interest, in units of photons/s; it is found by integrating the flux F as a function of λ taking into account the efficiency loss factors: the transmission coefficient of the atmosphere, of the telescope and of the filter, the quantum efficiency of the detector, and the fraction of the point spread function (*PSF*) falling inside the light-collecting aperture.

In the above equation the *noise* term is obtained as a term of N_{sky} (the total number of photons per pixel from the background or sky) and another one as n_{pixel} (the number of pixels under consideration) times the contributions from N_{dark} (the total number of dark-current electrons per pixel), and RON^2 (the total number of electrons per pixel resulting from the read noise⁽⁴⁾). *AntETC* may calculate S/N for a given time or t for a desired S/N value. It can also provide a graphical representation of S/N as a function of t so that users can understand if the CCD will saturate the frame.

3.1.1. Uncertainty on the magnitude as a function of S/N . Usually, uncertainties in astronomy are expressed using the logarithmic magnitude scale. In the following, we will consider the background terms as systematic uncertainties on the signal count rate. We converted S/N in magnitude by applying

$$(3) \quad (\text{mag}) \pm \Delta(\text{mag}) = (\text{mag})_0 - 2.5 \log_{10}(S \pm N).$$

So, it is easy to find that

$$(4) \quad \Delta(\text{mag}) \approx 1.086 \left(\frac{1}{S/N} \right).$$

4. – Calibration

This section shows the photometric zero points for the most frequently used (BVRcIc), a first determination of the color terms and the value of extinction coefficients. The UB filter was not used thus far.

4.1. Standard star fields and observation. – We used ~ 30 standard stars, taken from the Landolt catalogue [2]. Due to the 20×10 arcmin FoV of the CCD, we observed at the same time at most seven standard stars. With TOPCAT [3] we built a table of standard stars.

4.2. Data reduction. – We realized a series of custom-made Python programs, all inside the Antola telescope Graphical User Interface (*AntGUI*) to select automatically the photometric standard star observations obtained with the Antola Telescope. *AntGUI* uses IRAF⁽⁵⁾ task to reduce, align and combine all images. The images are dark subtracted and flat-field corrected.

4.3. Photometry. – The combined images were processed in order to determine the full width at half maximum (FWHM) and ellipticity ϵ of the PSF. The average value of FWHM was used to determine the aperture size to be used for the photometry. The aperture radius for each image is $4 \cdot \text{FWHM}$. The instrumental magnitudes m_{instr} were calculated as

$$(5) \quad m_{\text{instr}} = -2.5 \cdot \log_{10}(f) + 2.5 \cdot \log_{10}(t),$$

⁽⁴⁾ Note that this noise source is not a Poisson noise source but a shot noise; therefore it enters into the noise calculation as the value itself, not the square root of the value as Poisson noise sources do.

⁽⁵⁾ Image Reduction and Analysis Facility is a collection of software written at the National Optical Astronomy Observatory (NOAO) geared towards the reduction of astronomical images in pixel array form. You can freely download it from <http://iraf.noao.edu/>.

TABLE II. – *Experimental values of the extinction coefficient.*

Passband	$\bar{k}_\lambda \pm \sigma_k$ (mag/airmass)
<i>B</i>	0.742 ± 0.005
<i>V</i>	0.543 ± 0.002
<i>R</i>	0.463 ± 0.005
<i>I</i>	0.376 ± 0.005

where t is the exposure time of the frame and f is the total number of counts, excluding sky, in the aperture: $f = s - A \cdot M_{\text{sky}}$, where s the total number of counts including sky in the aperture, A is the area of the aperture in square pixels and M_{sky} the best estimate of the sky value (per pixel). The uncertainty on the instrumental magnitude is defined as the inverse of (S/N) . The calibrated magnitude M_{λ_1} , at a given passband, λ_1 , was derived as the sum of several components as follows:

$$(6) \quad M_{\lambda_1} = z_{\lambda_1} + m_{\lambda_1} - k_{\lambda_1} AM + c_{\lambda_1} (m_{\lambda_1} - m_{\lambda_2}),$$

where z_{λ_1} is the zero point of the photometric system at a given passband, m_{λ_1} is the instrumental magnitude, k_{λ_1} is the extinction coefficient, AM is the airmass at the observation time, c_{λ_1} is the color term and $m_{\lambda_1} - m_{\lambda_2}$ is the instrumental color index from two different filters. To find all parameters $(z_{\lambda_1}, k_{\lambda_1}, c_{\lambda_1})$ we studied separately the extinction coefficient and the zero point as follows.

5. – Results

5.1. Atmospheric extinction. – The standard stars were observed after passing the meridian. So for most of them the airmass $AM \simeq 1$. In order to determine the atmospheric extinction we observed a single field of standard stars (SA41) during a night and verified that a first-order approximation is more than enough. At the effective wavelength λ , the instrumental magnitude m_{instr} is related to the extra-atmosphere instrumental magnitude m_0 by Bouguer’s law

$$(7) \quad m = m_0 + k_\lambda AM,$$

where k_λ is the extinction coefficient (measured in mag/airmass). The automatic reduction of the data leads to the values reported in table II.

5.2. Zero point and color terms. – We use the following equation to find the zero point correction and the color term:

$$(8) \quad M_{\lambda_1} = z_{\lambda_1} + m + c_{\lambda_1} (m_{\lambda_1} - m_{\lambda_2}),$$

TABLE III. – *The zero points and the color term of the Johnson filters computed for the Antola Observatory.*

Equation	Zero points ($zp_\lambda \pm \sigma_{zp}$)	Color term ($c_\lambda \pm \sigma_c$)
(9a)	23.03 ± 0.06	-0.26 ± 0.12
(9b)	22.72 ± 0.03	0.04 ± 0.06
(9c)	22.73 ± 0.02	0.14 ± 0.13
(9d)	22.40 ± 0.04	0.56 ± 0.4
(9e)	22.63 ± 0.25	0.15 ± 0.19
(9f)	21.93 ± 0.40	0.90 ± 0.30

where now m is already corrected for the presence of the atmosphere, $m = m_{\lambda_1} - k_{\lambda_1} AM$. This equation can be written for every filter as

$$\begin{aligned}
 (9a) \quad & B - b = z_b + c_b(b - v), \\
 (9b) \quad & V - v = z_v + c_v(b - v), \\
 (9c) \quad & V - v = z_v + c_v(v - r), \\
 (9d) \quad & R - r = z_r + c_r(v - r), \\
 (9e) \quad & R - r = z_r + c_r(r - i), \\
 (9f) \quad & I - i = z_i + c_i(r - i),
 \end{aligned}$$

where the capitals letters are the expected magnitudes (theoretical magnitudes) of the standard stars, and lowercase letters are the instrumental magnitudes. We use the *k-folding method* to extract the values of the zero point and color term. Table III shows the values we obtained for the Antola Observatory. We tested these values observing a new set of standard stars and computing the differences between the real magnitudes and the calibrated magnitudes. The errors are smaller than 0.01 magnitude.

6. – First results

In this section two observing programmes are described: the transit of extrasolar planets and the variability of Weak Emission Line Quasars (WELQs).

6.1. Transit of exoplanets. – As a first attempt to assess the scientific reliability of the instrument, we observed the transit of an already known exoplanet: WASP58b. This is a transiting close-in giant planet observed for the first time in 2013 [4]. The observations of WASP-58b obtained at OARPAF helped to integrate other data taken at the 82 cm telescope built by the Instituto de Astrofísica de Canarias (called IAC-80) and the Carlos Sánchez Telescope (TCS) located in the IAC’s Teide Observatory (paper in preparation). In fig. 2 the preliminary light curves of two transits of WASP-58b obtained at OARPAF are shown.

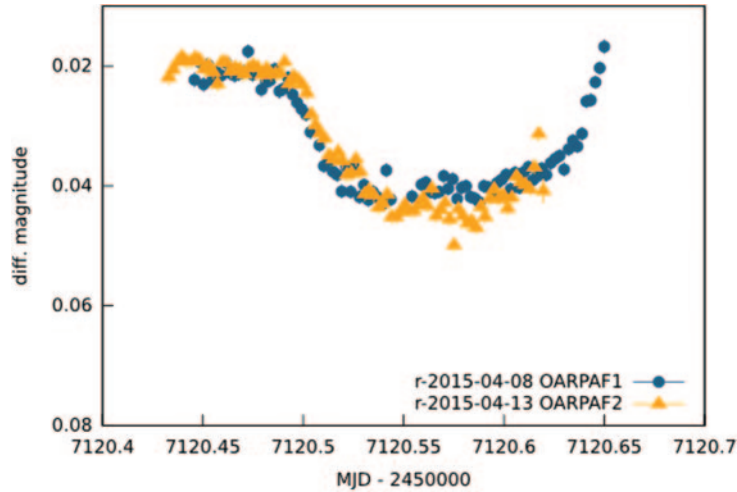


Fig. 2. – Preliminary light curves obtained for two transits of WASP-58b.

6.2. Variability of AGN. – Quasars are often characterized by prominent broad emission lines. However, during the last decade, quasars with weaker emission lines were found. Weak Emission Line Quasars (WLQs) are a recently discovered class of active galactic nuclei. As investigations of their spectra have shown, they share some properties of radio-quiet quasars but their optical and UV spectra lack strong emission lines. Most of such objects were found with high redshift ($z > 2.5$). WLQs were originally defined as quasars having $EW \leq 15.4 \text{ \AA}$ for the $\text{Ly}\alpha + \text{N}$ lines [5, 6]. A list of WLQ is found in [7]. Another class of objects is represented by *blazars*, AGN whose jet points to the observer [8].

To discriminate among models of WLQs, a possibility is to monitor the incident flux (or magnitude) over time.

- We will observe 14 WLQs included in the list of [7] in order to test the presence of large variability and determine the nature of these object (blazar or normal quasar (QSO)).
- If we observe low variability, we may compare it with the variability of the curves of normal QSO and test the accretion disk modelling.

First I made the feasibility study of the above mentioned measurement and then I took the first data: the whole campaign is expected to last about one year.

* * *

I am grateful to Filippo Zerbi, Luciano Nicastro, Eliana Palazzi, Massimo Ancona, Marco Pallavicini, Lorenzo Cabona for inputs in the preparation of this work. In particular, I thank Silvano Tosi, Andrea La Camera, Marco Landoni, Davide Ricci and Carlo Schiavi for useful suggestions, comments and for a careful reading of this paper.

REFERENCES

- [1] FEDERICI A., ARDUINO P., RIVA A. and ZERBI F. M., *Astron. Soc. India Conf. Series*, **7** (2012) 7.
- [2] LANDOLT. *et al.*, *Astron. J.*, **146** (2013) 131.
- [3] TAYLOR M. B., *TOPCAT & STIL: Starlink Table/VOTable Processing Software*.
- [4] HEBRARD G. *et al.*, *Astron. Astrophys.*, **549** (2013) A134.
- [5] BECKMANN V. and SHRADER C., *Active galactic nuclei* (WILEY-VCH, Germany) 2014, pp. 1–10.
- [6] LANDONI M. *et al.*, *Astron. J.*, **149** (2015) 163.
- [7] DIAMOND-STANIC ALEKSANDAR M. *et al.*, *Astrophys. J.*, **699** (2009) 782.
- [8] LANDONI M. *et al.*, *Astron. J.*, **145** (2013) 114.